MECHANOCHEMISTRY

Flyby reaction trajectories: Chemical dynamics under extrinsic force

Yun Liu[1,2], Soren Holm[3,4,5], Jan Meisner[3,4,5], Yuan Jia[1,2], Qiong Wu[1,2], Toby J. Woods[2,6], Todd J. Martinez[3,4,5]*, Jeffrey S. Moore[1,2]*

Dynamic effects are an important determinant of chemical reactivity and selectivity, but the deliberate manipulation of atomic motions during a chemical transformation is not straightforward. Here, we demonstrate that extrinsic force exerted upon cyclobutanes by stretching pendant polymer chains influences product selectivity through force-imparted nonstatistical dynamic effects on the stepwise ring-opening reaction. The high product stereoselectivity is quantified by carbon-13 labeling and shown to depend on external force, reactant stereochemistry, and intermediate stability. Computational modeling and simulations show that, besides altering energy barriers, the mechanical force activates reactive intramolecular motions nonstatistically, setting up "flyby trajectories" that advance directly to product without isomerization excursions. A mechanistic model incorporating nonstatistical dynamic effects accounts for isomer-dependent mechanochemical stereoselectivity.

Explanations of chemical reactivity are conventionally supported by statistical theories in chemical dynamics. In this classical picture, Boltzmann statistics are assumed to govern energy distributions on the potential energy surface and the corresponding rate constants. Consequently, product distributions are dictated by the relative frequencies with which energy barriers are surmounted among the competing intrinsic reaction coordinates. Emerging examples are challenging these perceptions by showing that even the outcomes of textbook organic reactions are influenced by nonstatistical dynamic effects (NDEs) (*1*–*3*). That is, the momenta (directions and speed) of the atoms in reacting species lessen the influence of Boltzmann statistics and lead to product distributions that depart from the statistical predictions (*4*–*8*). In some enzymes, NDEs are shown to steer reaction flux toward desired channels (*9*); on the benchtop, external controls over competing reaction paths have largely relied on the more conventional approach, modifying potential energy surfaces to affect relative rates (*10*–*13*). Extrinsic force is also known to modify potential energy surface to access reactivity and selectivity differently from their zero-force counterparts (*14*, *15*), enabling thermally forbidden trajectories (*16*), shifting chemical equilibria (*17*, *18*), and stabilizing otherwise fleeting intermediates (*19*). The acceleration of bond reorganization by force to promote nonequilibrium energy distributions inspired us to postulate that the extrinsic force can impose and control NDEs to steer reaction trajectories away from Boltzmann statistics even on the already force-modified potential energy surface (FMPES). It was recently observed that nonstatistical chemical dynamics can occur in mechanochemical reactions (*20*–*22*). However, the extent to which these trajectories are nonstatistical on the FMPES, and in particular, whether the nonstatistical behaviors are tunable by the extrinsic force are not known.

To investigate the postulated role of force in inducing and controlling NDEs, we chose a cyclobutane ring-opening reaction that follows a stepwise mechanism (*23*–*25*), is mechanochemically active (*25*–*27*), and exhibits a distribution of stereoisomeric products (*20*, *27*, *28*). The product's stereochemistry is determined after passing over the rate-limiting barrier of the first bond scission; from there, competing isomerization channels branch from the initially formed diradical intermediate (Fig. 1A). The reaction either proceeds directly to complete the ring opening with the second bond scission, or the intermediate undergoes isomerization before the second bond scission transpires. Owing to the instability of the diradical intermediates (*24*), the stereo-defining events are not expected to be rate-limiting under force. Consequently, on this FMPES, force-controlled NDEs can govern pathway selection by outpacing thermal equilibration of the diradical intermediate at the branch point. The resulting product stereoselectivity serves as a sensitive reporter of force-controlled NDEs.

We hypothesized that momenta derived from the extrinsic force can propel trajectories to "fly by" the isomerization branch points and thereby achieve nonstatistical product distribution even on the FMPES. Such flyby trajectories traverse the energy landscape via excited vibrational energy levels of the diradical intermediate without undergoing relaxation (Fig. 1B). Atomic motions associated with flyby trajectories are thus accelerated beyond their thermal rates, altering selectivity that is intrinsic to the FMPES such that the resulting product stereochemistry directly relates to the stereochemistry of the reactant. In contrast, deepening the potential well at the branch point increases the likelihood of vibrational relaxation, restoring the statistical reaction outcome of the FMPES.

To test our hypothesis, we designed and synthesized a series of cyclobutane stereoisomers from the stereoselective [2σ + 2σ + 2π] cycloaddition (*29*) between quadricyclane and ^{13}C-labeled alkenes (Fig. 2A). The alkyl and ester substituents offer different diradical stability (table S4) to vary the depth of the potential well at the branch point. The stereochemistry of the cyclobutanes was confirmed by spatial proximity of protons (figs. S1 to S4) and x-ray crystal structures (Fig. 2B). These isomers are denoted as *anti* (**A**), *down* (**D**), and *up* (**U**) following the orientations of substituents. Using the constrained geometries simulate external force (CoGEF) calculation (figs. S9 to S16), an ab initio energy-extension modeling method, all designed cyclobutane stereoisomers were predicted to undergo mechanically activated retro-[2+2] cycloaddition (*30*). Cu(0)-mediated radical polymerization was carried out from the initiator-bearing cyclobutanes using methyl acrylate (Fig. 2C) to render linear polymers of controlled molecular mass (M_n): 40 to 140 kDa, $Đ$ < 1.2 (figs. S19 to S23). The well-controlled bidirectional polymerization allowed for statistically chain-centered placement of cyclobutanes in the polymer chain while retaining high stereochemical purity (figs. S23 to S27).

We experimentally evaluated the mechanochemistry by sonication-induced solvodynamic extension of polymer chains (fig. S28) (*31*), and the resulting solutions were characterized by ^{13}C nuclear magnetic resonance (NMR) spectroscopy. For the alkyl-substituted cyclobutanes, sonication resulted in new ^{13}C-labeled methylene ($^{13}CH_2$) and alkene methine (^{13}CH) peaks at δ = ~60 and ~120 parts per million (ppm), respectively (Fig. 3A and figs. S29 to S31). The coupling between the methylene and alkene peaks (table S5) suggests ring opening of cyclobutanes into alkenes. On the basis of the three distinctive alkene peaks, reference compounds (fig. S34), and calculated ^{13}C chemical shifts (table S6), we assigned the ring-opening product of the **A**-isomer to an (*E*,*Z*)-bisalkene, the **D**-isomer to an (*E*,*E*)-bisalkene, and the **U**-isomer to a mixture of (*Z*,*Z*)- and (*E*,*Z*)-bisalkenes in an 8:1 ratio. The observation of

[1]Beckman Institute for Advanced Science and Technology, University of Illinois at Urbana-Champaign, Urbana, IL 61801, USA. [2]Department of Chemistry, University of Illinois at Urbana-Champaign, Urbana, IL 61801, USA. [3]Department of Chemistry, Stanford University, Stanford, CA 94305, USA. [4]The PULSE Institute, Stanford University, Stanford, CA 94305, USA. [5]SLAC National Accelerator Laboratory, 2575 Sand Hill Road, Menlo Park, CA 94025, USA. [6]3M Materials Chemistry Laboratory, School of Chemical Sciences, University of Illinois at Urbana-Champaign, Urbana, IL 61801, USA.
*Corresponding author. Email: todd.martinez@stanford.edu (T.J.M.); jsmoore@illinois.edu (J.S.M.)

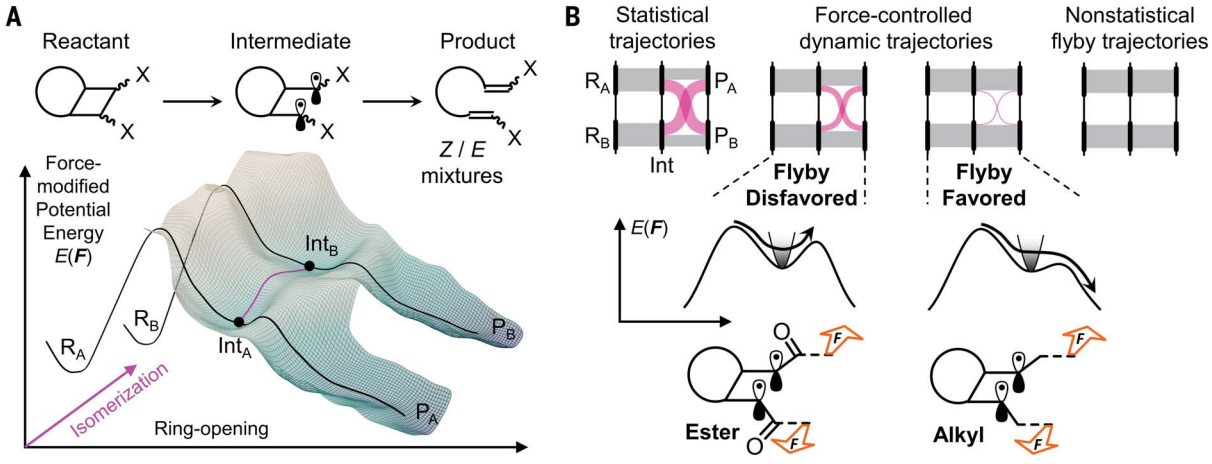

Fig. 1. Nonstatistical dynamic effects induced by extrinsic force. (**A**) A generic force-modified potential energy landscape for stepwise ring opening of isomeric cyclobutane reactants R_A and R_B. (**B**) The force-induced NDE hypothesis represented schematically by alluvial flow diagrams. Colored flows: gray, reaction trajectories that ring-open without undergoing isomerization; magenta, reaction trajectories that isomerize and then ring-open.

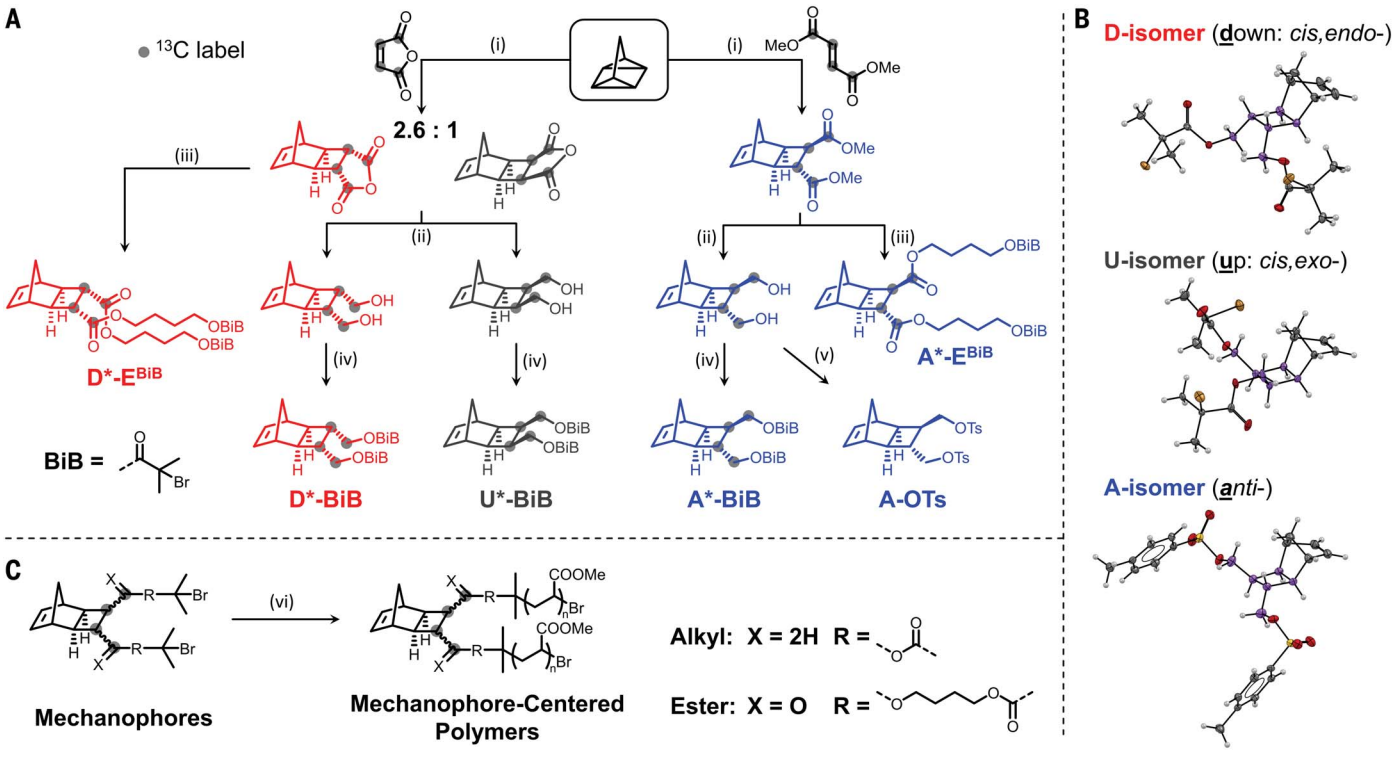

Fig. 2. ^{13}C-labeled cyclobutane mechanophores. (**A**) Synthesis, (**B**) stereochemical validation, and (**C**) polymer synthesis. Reaction conditions: (i) PhMe, 110°C. (ii) $LiAlH_4$, THF, 0°C. (iii) KOH or LiOH; then 4-hydroxybutyl 2-bromoisobutyrate, EDCI•HCl, DMAP, THF. (iv) BiB-Br, Et_3N, THF. (v) TsCl, Et_3N, THF (a nonlabeled reactant was used). (vi) Methyl acrylate, Cu(0), Me_6TREN, DMSO. THF, tetrahydrofuran; EDCI, *N*-(3-dimethylaminopropyl)-*N*′-ethylcarbodiimide; DMAP, *N*,*N*-dimethylaminopyridine; Ts, 4-4-methylsulfonyl (tosyl); Me_6TREN, tris[2-(dimethylamino)ethyl]amine; DMSO, dimethylsulfoxide. Color coding in (B): carbon, gray; oxygen; red; bromine, brown; sulfur, yellow; hydrogen, white; cyclobutane ring and its α-CH_2 carbon, violet. All thermal ellipsoids are shown at 50% probability.

(*E*,*Z*) by-product from the **U**-isomer suggests that the two radicals behave independently after generation, confirming the stepwise mechanism. Despite being stepwise, the ring opening of the alkyl cyclobutanes achieved high stereoselectivity. This conservation of stereochemical information suggests that the force-imparted momentum and/or force-modified energy landscape is effective in steering the reaction trajectories away from excursions at downhill branch points (Fig. 1B).

We then turned to the ester-substituted cyclobutanes, which stabilize the diradical intermediates more than the alkyl derivatives. Under the same sonication conditions, mechanochemical production of α,β-conjugated diesters was observed for the **A**- and **D**-isomer (fig. S33); the **U**-isomer was not obtained because of isomerization during synthesis and was not experimentally studied. NMR analysis of carbon multiplicity (number of attached protons), spin-spin coupling, and alkene stereochemistry using the ^{13}C-labeled product peaks (fig. S35 and tables S5 and S7) revealed considerably

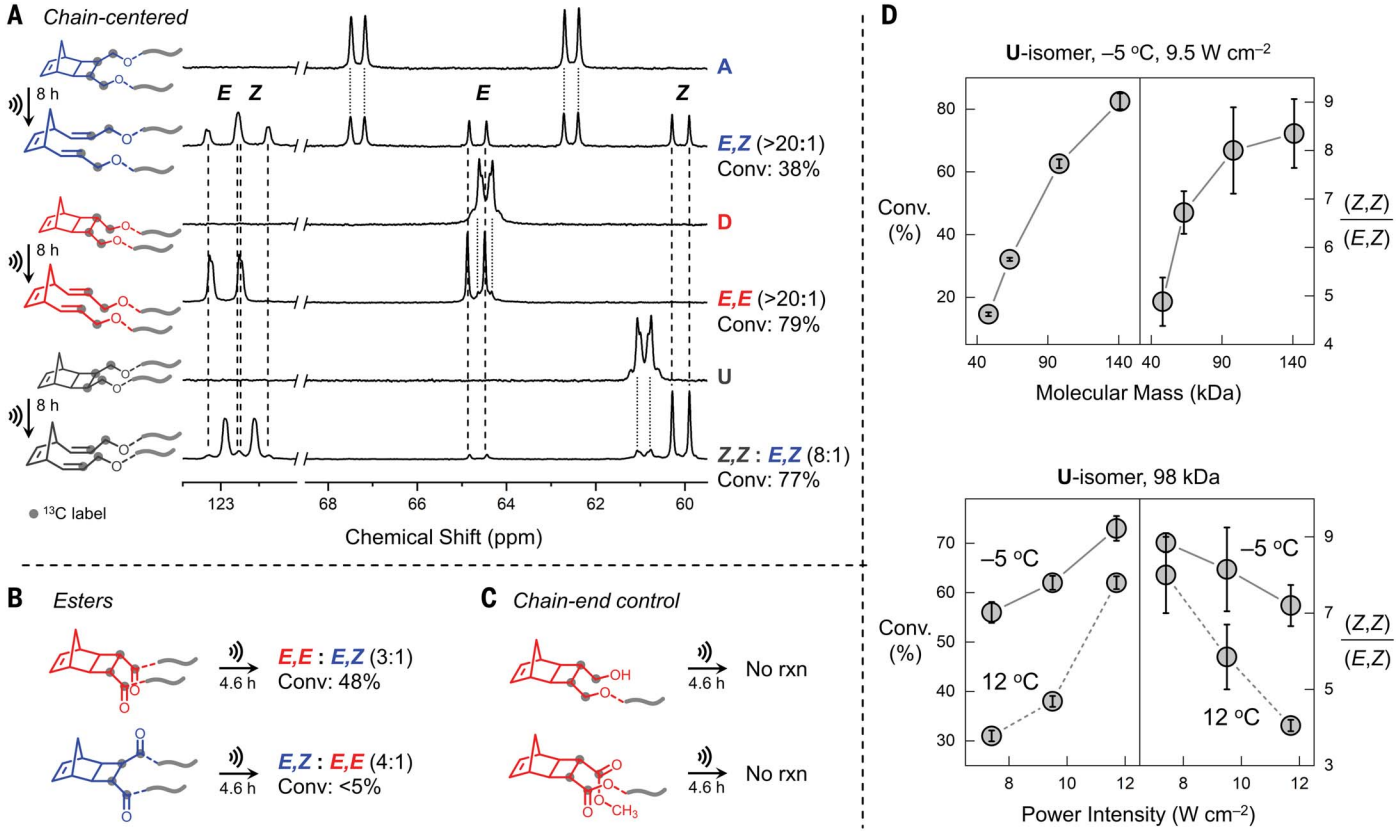

Fig. 3. Mechanochemical activation of cyclobutanes. (**A**) Stacked ^{13}C NMR spectra of chain-centered alkyl cyclobutanes in a ~100-kDa polymer before and after sonication (20 kHz, 9.5 W/cm^{-2}, –5°C, THF). (**B**) Mechanochemical activation of chain-centered ester variants. (**C**) Attempted mechanochemical activation of chain-end control cyclobutanes. (**D**) Impact of experimental variables on the conversion and product selectivity for the alkyl **U**-isomer. Errors are presented in 2σ from four measurements of relative integrations by using the two pairs of ^{13}C NMR peaks.

lower stereoselectivity (Fig. 3B). The preferred alkene geometry remained the same as for the alkyl variants, but the selectivity fell from >20:1 to ~3:1. Loss of stereoselectivity arises from torsional rotations that occur via the diradical states, e.g., the **A**-isomer produces the (*E*,*E*)-bisalkene after the upward substituent rotates downward. The reduced stereoselectivity of ester variants suggests that force-driven dynamics compete less effectively with bond rotations when the there is a deeper energy well associated with the intermediate (Fig. 1B).

Mechanochemical activation was not observed in chain-end control polymers (Fig. 3C) in which nearly no force is exerted on the cyclobutanes. Nor did heating at 240°C result in any conversion (figs. S38 and S39), suggesting a pronounced rate acceleration by extrinsic force on high-barrier thermal reactions. We used relative integrations of the α-$^{13}CH_2$ carbon peaks to quantify the mechanochemical conversion of alkyl derivatives within a ~100-kDa polymer (figs. S43 to S46). The data were best-fitted with a competing first-order kinetics model to account for both activation and background polymer scission to obtain conversion rates (fig. S47). The **D**-isomer displayed the fastest conversion of 0.46 hour^{-1}, followed by the **U**-isomer (0.31 hour^{-1}) and then the **A**-isomer (0.14 hour^{-1}), consistent with the rank order of predicted rupture force by CoGEF (table S4) and literature precedents (*32*).

To alter the mechanochemical reaction outcomes, we explored a range of experimental variables (Fig. 3D) on the alkyl cyclobutanes. Our screening initially focused on the **U**-isomer as the test compound. Conversions were improved with increasing sonication-induced extensional force, by using longer polymers (fig. S52), lower solution temperatures, or higher ultrasound intensities (fig. S54) (*33*). The stereoselectivity of the **U**-isomer exhibited a positive dependence on force when molar masses and solution temperatures were changed, but a negative dependence on force-loading rate when ultrasound intensity was increased (eq. S1). Exploring the known effect of experimental variables, we altered the product ratios between the (*Z*,*Z*) and the (*E*,*Z*)-bisalkenes for the alkyl **U**-isomer from 4:1 to 10:1 (fig. S55). In comparison, the high stereoselectivities of the **A**-isomer and **D**-isomer persisted under all conditions (fig. S55), suggesting that force-imparted dynamics are isomer dependent.

We reasoned that the force-induced dynamics are bound by two limits. First, there is a thermal limit that reflects the statistical reaction outcome based on the FMPES; the imparted momenta largely dissipate by thermal relaxation. Second, there is a dynamic limit that reflects the experimentally achievable nonstatistical selectivity. Although experimentally we observed the nonstatistical outcome anticipated from our design, a theoretical investigation is necessary to quantify the dynamic and thermal contributions.

To characterize the thermal limit, we computationally mapped out the force-modified minimum energy paths (MEPs) for alkyl cyclobutanes using acetyl-terminated model compounds (Fig. 4A). When the pulling force was varied from 1 to 2 nN, energy barriers of the second scissions were lowered by 2 to 3 kcal mol^{-1} and those of isomerizations were raised by 3 to 4 kcal mol^{-1} (Fig. 4B). The mode selection is consistent with the coupling between force and reactive molecular extension during ring opening, whereas force-resistive contraction was seen during isomerization. Among the three isomers, **U** had the lowest isomerization barriers that became disfavored beyond 1.3 nN. At this cross-over point, we constructed a full FMPES using 470 ab initio steered molecular dynamics (AISMD) trajectories

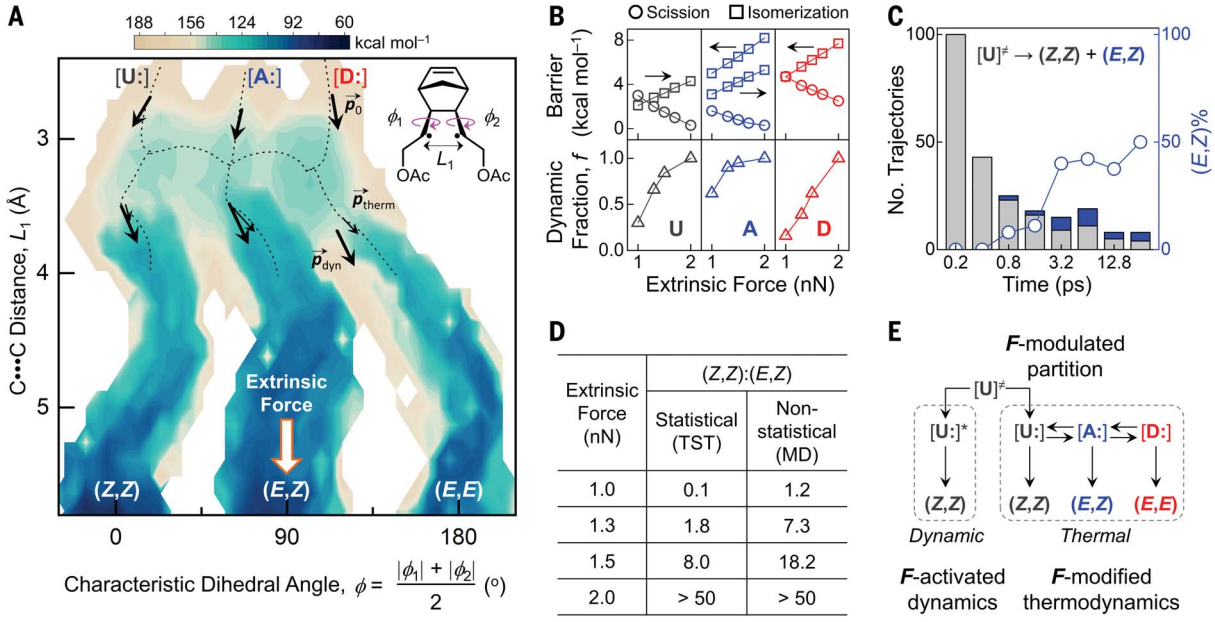

Extrinsic Force (nN)	(Z,Z):(E,Z)	
	Statistical (TST)	Non-statistical (MD)
1.0	0.1	1.2
1.3	1.8	7.3
1.5	8.0	18.2
2.0	> 50	> 50

Fig. 4. Nonstatistical dynamics of cyclobutane ring opening under extrinsic forces. (**A**) FMPES constructed from AISMD (1.3 nN, 300 K) runs on model compounds; [**X:**] indicates the diradical intermediates. The extension coordinate (L_1) was chosen to represent bond scissions during ring opening, and the dihedral coordinate (ϕ, magenta) was chosen for isomerization. Dashed lines depict the MEPs. Colored arrows represent time- and ensemble-averaged reaction momenta over a 20-fs interval: thick black, entrance momenta $\vec{p}_0$ and dynamic exit momenta $\vec{p}_{dyn}$; thin black, thermalized exit momenta $\vec{p}_{therm}$. The orange, hollow arrow indicates that the direction of the extrinsic force is parallel to the ring-opening L_1 axis. (**B**) Top: Free energy barriers of the second C–C bond scission and diradical isomerization. Arrows indicate directions of isomerization along the **U**-**A**-**D** path. Bottom: Force-dependent partition coefficient (*f*) of dynamic trajectories. (**C**) Histogram of MD trajectories for **U** at 1.3 nN. $[U]^{\neq}$ indicates the first-bond scission transition state. (**D**) Statistical (TST) and nonstatistical (MD) product selectivity under different extrinsic forces. (**E**) Hybrid NDE model exemplified by the ring opening of **U**. [**U:**]* indicates vibrationally excited diradical intermediates of the **U**-isomer.

initialized from the rate-limiting transition states of the three isomers (Fig. 4A). The result features three ring-opening paths running downhill to the bisalkene products. The diradical intermediates were characterized as shallow calderas separated by isomerization barriers. The intermediate from **U** is less stable than the intermediate from **D**, raising the isomerization probability of the intermediate from **U**.

We garnered ~1000 force-steered MD trajectories (table S12) to study the force-induced dynamic effects. Exemplified by **U**, we saw that a large reaction flux flies by the branch areas at early simulation times (<0.5 ps) with a strong preference for the direct ring-opening channel and conservation of reactant stereochemistry (Fig. 4C, figs. S79 to S81, and movie S5). Over time, the force-imparted reaction momenta relax and isomerization ensues in conformity with the FMPES; this temporal distribution of product formation and selectivity are hallmarks of NDEs (*34*, *35*). The partition of trajectories into dynamic and thermal regimes resulted in bimodal rates of decay for the population of intermediates from the branch points (fig. S82). The fraction of dynamic trajectories (*f*) increased with increasing force for all three isomers but in an isomer-dependent manner: **A** > **U** > **D** (Fig. 4B); at 1.3 nN, dynamic trajectories make up 90, 66, and 39% of the total trajectories for **A**, **U**, and **D**, respectively. This dependence mirrors the rank order of their second scission barrier heights, supporting the prediction that a deeper potential well at the branch point reduces the number of dynamic trajectories.

To quantify the dynamic effects, we extracted atomic reaction momenta ($\vec{p}$) from the MD trajectories (Fig. 4A and table S13). An ensemble-averaged momentum characterizes the mean velocity and direction of the trajectories on the FMPES. In the dynamic regime (t < 0.5 ps), the momenta ($\vec{p}_{dyn}$) of trajectories exiting the branch areas deviate noticeably from the MEPs, showing a tendency to align with the extrinsic force. In contrast, the exit momenta in the thermal regime ($\vec{p}_{therm}$; t > 1 ps) closely adhered to the MEPs. The projected momenta on the extension coordinate (L_1, Fig. 4A) were fully conserved through the branch points, as shown by comparing the maximal momenta coming into and out of the areas; $\vec{p}_0$ and $\vec{p}_{dyn}$, respectively. The minimal loss in velocity along L_1 suggests little to no equilibration of the diradical intermediate in the dynamic regime, a signature of flyby trajectories. The force-derived momenta imparted to reactants on flyby trajectories were quantified by vector subtraction between dynamic and thermal exit momenta (fig. S91). We saw that the extrinsic force accelerates the atomic velocity of reactive molecular extension to 200% of their thermal values, reaching ~1.4 nm/fs (T_{eff} ~ 1000 K). In contrast, no consistent changes were observed for the dihedral coordinate between dynamic and thermal regimes, and their average angular velocity (8.5°/fs) is the same as in the competing isomerization trajectories. This distinction reveals that the extrinsic force selectively activates the chemical dynamics of reactive molecular extensions (Fig. 1B) over isomerization, leading to nonstatistically enhanced product stereoselectivity (Fig. 4D and fig. S95). At 1.3 nN, the NDEs improve product selectivity by fourfold for **U** in comparison to the statistical outcome. The apparent enhancement on selectivity is much smaller (<10%) for **A** and **D**, because of **A** being a kinetic trap and an already preferred product channel on the FMPES and **D** having a relatively low dynamic contribution (Fig. 4B).

The isomer-dependent dynamic responses result from a varying degree of openness in the exit reaction channels along the dihedral coordinate, which is further determined by reactant stereochemistry (fig. S92). The 120° ridge on the FMPES blocks the majority of dynamic exit coming from **D**, leaving behind a narrow and risen gorge (Δϕ = 3°) for its thermal exit (Fig. 4A). In contrast, the exit channel for **A**

is wider ($\Delta\phi$ = 45°), whereas for **U** there is a modest constriction ($\Delta\phi$ = 35°). We used an additive model to relate dynamic population (*f*) and the relative configuration of stereocenters on the cyclobutane rings. Mathematically, we found that the stereochemistry along the pulling direction plays a primary role in promoting dynamic trajectories, with trans configuration much better than cis; the stereochemistry orthogonal to the force is secondary, with cis better than trans. This rule allowed us to rank the tendency to undergo dynamic ring opening for all possible cyclobutane stereoisomers (fig. S93).

The force-induced NDE is expressed as a linear hybridization of dynamic and thermal extremes with a force-dependent partition (Fig. 4E). The dynamic regime is stereospecific by definition, and the selectivity of product isomers in the thermal regime was assumed to be statistical. This statistical (transition state theory, TST) stereoselectivity (S_{TST}) was obtained from equilibrium product distributions calculated by solving the system of rate equations of the activation-isomerization reaction network (Fig. 4E, right box, and fig. S94). The rate constant for each rate equation was calculated by TST (table S14). The force-dependent nonstatistical stereoselectivity (S_{NDE}), defined as the ratio between direct stereoisomeric product and all isomerization products, is predictable from the statistical stereoselectivity, S_{TST}, and the dynamic fraction, *f*:

$$S_{NDE} = \frac{S_{TST} + f}{1 - f} \quad (1)$$

When the dynamic fraction increases from 0 to 1, the S_{NDE} goes from its thermal value, S_{TST} (f = 0), to being a stereospecific transformation in the limit when $f \rightarrow 1$ (table S15). This model reproduces the observed dynamic selectivity without the need to run full long MD simulations.

The hybrid NDE framework reveals that there is not necessarily a simple connection between the intermediate's stability and the dynamic selectivity of mechanochemical reactions. Although the stereoconvergent ring opening of the ester-substituted cyclobutane has been observed and attributed to its long-living intermediate (*28*), our study suggests that a long-lived intermediate need not be destined for lower stereoselectivity. Indeed, we have improved the product stereoselectivity of the ester derivatives compared to the reported literature values. Similarly, the alkyl **D**-isomer displayed high stereoselectivity under all experimental conditions despite its longest diradical lifetime as shown by radical quenching experiments with 4-hydroxyl TEMPO (table S17). Rather, stereoselectivity can be affected dynamically for a short-lived intermediate: for example, by a neighboring product channel serving as a dynamic sink to draw the trespassing trajectories into an irreversible path, similar to the formation of (*E*,*Z*)-bisalkene from the **U**-isomer.

We envision that external force is an experimental method for controlling nonstatistical dynamics and steering reaction trajectories away from constraints imposed by potential energy surfaces. The hybrid framework will offer ability to probe and understand the dynamic effects of mechanochemical phenomena in polymeric materials. The ability to control dynamics and stereochemistry of mechanochemical reactions may be helpful for programming properties of next-generation polymeric materials whose life cycles will go beyond the single-use paradigm.

REFERENCES AND NOTES

1. B. K. Carpenter, *J. Am. Chem. Soc.* **117**, 6336–6344 (1995).
2. S. C. Ammal, H. Yamataka, M. Aida, M. Dupuis, *Science* **299**, 1555–1557 (2003).
3. Y. Nieves-Quinones, D. A. Singleton, *J. Am. Chem. Soc.* **138**, 15167–15176 (2016).
4. C. Doubleday, C. P. Suhrada, K. N. Houk, *J. Am. Chem. Soc.* **128**, 90–94 (2006).
5. F. F. Crim, *Proc. Natl. Acad. Sci. U.S.A.* **105**, 12654–12661 (2008).
6. J. Rehbein, B. K. Carpenter, *Phys. Chem. Chem. Phys.* **13**, 20906–20922 (2011).
7. J. Rehbein, B. Wulff, *Tetrahedron Lett.* **56**, 6931–6943 (2015).
8. S. R. Hare, D. J. Tantillo, *Pure Appl. Chem.* **89**, 679–698 (2017).
9. Y. J. Hong, D. J. Tantillo, *Nat. Chem.* **6**, 104–111 (2014).
10. J. Wang, B. L. Feringa, *Science* **331**, 1429–1432 (2011).
11. C. J. Brown, F. D. Toste, R. G. Bergman, K. N. Raymond, *Chem. Rev.* **115**, 3012–3035 (2015).
12. A. C. Aragonès *et al.*, *Nature* **531**, 88–91 (2016).
13. W. Mtangi *et al.*, *J. Am. Chem. Soc.* **139**, 2794–2798 (2017).
14. M. T. Ong, J. Leiding, H. Tao, A. M. Virshup, T. J. Martínez, *J. Am. Chem. Soc.* **131**, 6377–6379 (2009).
15. P. Dopieralski *et al.*, *Nat. Chem.* **5**, 685–691 (2013).
16. C. R. Hickenboth *et al.*, *Nature* **446**, 423–427 (2007).
17. A. E. M. Beedle *et al.*, *Nat. Commun.* **9**, 3155 (2018).
18. M. E. McFadden, M. J. Robb, *J. Am. Chem. Soc.* **141**, 11388–11392 (2019).
19. J. M. Lenhardt *et al.*, *Science* **329**, 1057–1060 (2010).
20. Z. Chen *et al.*, *Nat. Chem.* **12**, 302–309 (2020).
21. R. Nixon, G. De Bo, *Nat. Chem.* **12**, 826–831 (2020).
22. M. Wollenhaupt, C. Schran, M. Krupička, D. Marx, *ChemPhysChem* **19**, 837–847 (2018).
23. E. Fischer, R. Gleiter, *Tetrahedron Lett.* **26**, 5289–5290 (1985).
24. S. Pedersen, J. L. Herek, A. H. Zewail, *Science* **266**, 1359–1364 (1994).
25. M. J. Kryger *et al.*, *J. Am. Chem. Soc.* **132**, 4558–4559 (2010).
26. H. M. Klukovich, Z. S. Kean, S. T. Iacono, S. L. Craig, *J. Am. Chem. Soc.* **133**, 17882–17888 (2011).
27. Z. Chen *et al.*, *Science* **357**, 475–479 (2017).
28. Z. S. Kean, Z. Niu, G. B. Hewage, A. L. Rheingold, S. L. Craig, *J. Am. Chem. Soc.* **135**, 13598–13604 (2013).
29. I. Tabushi, K. Yamamura, Z. Yoshida, *J. Am. Chem. Soc.* **94**, 787–792 (1972).
30. I. M. Klein, C. C. Husic, D. P. Kovács, N. J. Choquette, M. J. Robb, *J. Am. Chem. Soc.* **142**, 16364–16381 (2020).
31. P. A. May, J. S. Moore, *Chem. Soc. Rev.* **42**, 7497–7506 (2013).
32. M. J. Kryger, A. M. Munaretto, J. S. Moore, *J. Am. Chem. Soc.* **133**, 18992–18998 (2011).
33. J. M. Lenhardt, A. L. Black Ramirez, B. Lee, T. B. Kouznetsova, S. L. Craig, *Macromolecules* **48**, 6396–6403 (2015).
34. B. K. Carpenter, *Chem. Rev.* **113**, 7265–7286 (2013).
35. D. R. Glowacki, S. P. Marsden, M. J. Pilling, *J. Am. Chem. Soc.* **131**, 13896–13897 (2009).

ACKNOWLEDGMENTS

Y.L. thanks J. Fu and X. Zhu for the helpful discussions. We thank O. Davydovich and D. Loudermilk for figure designs, and the SCS NMR Lab for its technical support. **Funding:** This work was supported by the National Science Foundation (NSF-CMMI-19-33932). T.J.M. and S.H. thank the Army Research Office (W911NF-15-1-0525) for financial support. J.M. thanks the Dr.-Leni-Schöninger foundation and the Deutsche Forschungsgemeinschaft (no. 419817859) for financial support. This work used the XStream computational resource supported by the National Science Foundation Major Research Instrumentation program (ACI-1429830). **Author contributions:** Y.L. conceived this work and performed synthesis and sonication experiments; S.H. performed dynamic simulations to construct the energy surfaces and reaction momenta; J.M. calculated the paths and the rate constants; Y.L., J.M., and S.H. interpreted the data and built the hybrid model; Y.J. assisted in the synthesis and sonication instrumentation; Q.W. assisted in polymer characterizations; T.W. performed x-ray structural analysis; T.J.M. and J.S.M. supervised the project; Y.L., T.J.M., and J.S.M. wrote the manuscript with input from all authors. **Competing interests:** The authors declare no competing interests. **Data and materials availability:** Crystallographic data are available free of charge from the Cambridge Crystallographic Data Centre under reference CCDC nos. 2051124, 2051125, and 2051126. All other data supporting the findings of this study are presented in the main text or supplementary materials.

SUPPLEMENTARY MATERIALS

science.sciencemag.org/content/373/6551/208/suppl/DC1
Materials and Methods
Supplementary Text
Figs. S1 to S100
Tables S1 to S17
References (*36*–*62*)
Movies S1 to S5
Structures

29 March 2021; accepted 3 June 2021
10.1126/science.abi7609

Flyby reaction trajectories: Chemical dynamics under extrinsic force

Yun Liu, Soren Holm, Jan Meisner, Yuan Jia, Qiong Wu, Toby J. Woods, Todd J. Martinez and Jeffrey S. Moore

Science **373** (6551), 208-212.
DOI: 10.1126/science.abi7609

Shear selectivity

Chemical reactions typically proceed by distributing energy statistically among all accessible molecular vibrations. Liu *et al.* report that external shear forces can sometimes pry open strained carbon rings without dissipating energy into adjacent bond rotations. Through careful design and synthesis of polymer-embedded cyclobutyl rings, the authors showed that certain relative substituent geometries are preserved when sonication induces ring opening. Accompanying simulations support the instigation of "flyby" trajectories that channel energy narrowly to cleave the cyclic sigma bonds and then rapidly form acyclic pi bonds.

Science, abi7609, this issue p. 208